A hydrophobic-hydrophilic MXene/PVDF composite hollow fiber membrane with enhanced antifouling properties for seawater desalination

Tao Zhang [a], Xin Guo [a], Brusly Solomon [b], Mohsen Sharifpur [c,d], Li-Zhi Zhang [a,*]

[a] Key Laboratory of Enhanced Heat Transfer and Energy Conservation of Education Ministry, School of Chemistry and Chemical Engineering, South China University of Technology, Guangzhou, 510640, China
[b] Micro and Nano Heat Transfer Lab, Centre for Research in Material Science and Thermal Management, Department of Mechanical Engineering, Karunya Institute of Technology and Sciences, Coimbatore, India
[c] Department of Mechanical and Aeronautical Engineering, University of Pretoria, Pretoria, 0002, South Africa
[d] Department of Mechanical Engineering, University of Science and Culture, Tehran, Iran

ARTICLE INFO

Keywords:
Desalination
Hollow fiber membrane
Antifouling
Antiwetting
Humidification

ABSTRACT

Hollow fiber membrane-based humidification-dehumidification desalination of seawater is a low-carbon freshwater-harvesting technology that can be powered by low-grade solar energy. Polyvinylidene fluoride (PVDF) can be easily fabricated into membranes and is considered the most promising material for industrial seawater desalination. However, membrane fouling and wetting have always been major obstacles with this technology. In this study, a hydrophobic-hydrophilic MXene/PVDF composite hollow fiber membrane (PVDF-MP) with remarkable antiwetting and antifouling properties was successfully prepared using a chemical grafting method. The interfacial dehydration reaction between the hydrophilic substrate layer (PVDF-OH) and the hydrophobic skin layer (MXene-P [MP]) was verified by Fourier-transform infrared spectroscopy and X-ray photoelectron spectroscopy, and a detailed reaction mechanism was provided. The hydrophilic substrate layer decreased moisture transfer resistance, while the hydrophobic skin layer reduced the membrane surface energy and increased the surface roughness. This resulted in a contact angle of 156.2°, which was measured using a new method that accounted for the curvature of the membrane. The superhydrophobic surface possessed a strong repulsive force toward water, and the air gap between the water and membrane impeded pollutant deposition on the inner surface of the membrane. Moreover, the rough surface created high entry pressure and prevented water from entering the membrane pores. Thus, the permeate flux of the PVDF-MP membrane persisted over 120 h during desalination tests, surpassing the performance of traditional materials.

1. Introduction

Membrane-based air humidification-dehumidification desalination (MHDD) is a thermally driven membrane separation technology that relies on humidification and dehumidification processes. This approach is widely used for desalination owing to several advantages including its mild operating conditions, high salt rejection rates, cost-effectiveness, and the high-quality water it produces [1,2]. More importantly, this technique has a low carbon footprint and can be powered by low-grade solar energy. The key component of MHDD systems is a hydrophobic membrane, which acts as a phase barrier to ensure high retention of nonvolatile substances [3,4]. Among the hydrophobic polymer materials, polyvinylidene fluoride (PVDF) has been widely used because of its strong thermal stability, inherent hydrophobicity [5], and ease of membrane fabrication. Flat sheet and hollow fiber modules are the main types of PVDF membrane modules. Compared to flat sheet modules, PVDF hollow fiber modules are more desirable for industrial applications owing to their self-supporting structure and high packing density [6]. Nevertheless, this module type undergoes fouling and wetting, and can be difficult to maintain and clean [7,8]. Over the past decade, improving surface hydrophobicity has been an area of increasing research interest [9–11]. Rezaei et al. [12] described the progress of superhydrophobic membrane antiwetting; when water droplets come into contact with a superhydrophobic surface, the water forms a convex meniscus owing to its high surface tension, thereby limiting water penetration through the membrane holes. On the other hand, Xiao et al. [10] identified the scaling resistance mechanism of superhydrophobic membranes. When a liquid dynamically flows over a superhydrophobic membrane, the interaction between the liquid and membrane is

* Corresponding author.
E-mail address: Lzzhang@scut.edu.cn (L.-Z. Zhang).

Nomenclature

m	mass (kg)
r	pore radius (m)
P	pressure (Pa)
P_{atm}	atmospheric pressure (Pa)
L	module length (m)
W	module wide (m)
H	module height (m)
d	fiber diameter (m)
P_L	longitudinal pitch (m)
P_T	transverse pitch (m)
P_D	diagonal pitch (m)
n_f	number of fibers
A_v	packing density (m^2/m^3)
A	membrane area of the module (m^2)
D_{ws}	water diffusivity in saline water (m^2/s)
D_{va}	moisture diffusivity in air (m^2/s)
D_{vm}	moisture diffusivity in membrane (m^2/s)
Nu	Nusselt number
Re	Reynolds number
Sh	Sherwood number
Pr	Prandtl number
Sc	Schmidt number
RH	relative humidity (%)
T	temperature (K)
u	velocity (m/s)
V_a	volume flow rate of the air (m^3/h)
V_s	volume flow rate of the saline water (mL/min)
x_s	molality of the feed side solution (mol NaCl/kg solution)
J	permeate flux ($kg/(m^2 \cdot h)$)
k	mass transfer coefficient (m/s)
M	molar mass (g/mol)
LEP_w	liquid entry pressure (kPa)

Greek letters

ε	porosity
δ	thickness (m)
ρ	density (kg/m^3)
θ	contact angle (°)
γ_L	liquid surface tension (N/m)
φ	packing fraction
ω	moisture content (kg moisture/kg air)
ν	kinematic viscosity (m^2/s)
γ_w	activity coefficient of water

Subscripts

a	air
s	saline water
tot	total
lm	logarithmic mean
m	membrane
p	permeate side
f	feed side
v	vapor
w	water
i	inlet
o	outlet
max	maximum value
m1	substrate layer in membrane
m2	skin layer in membrane

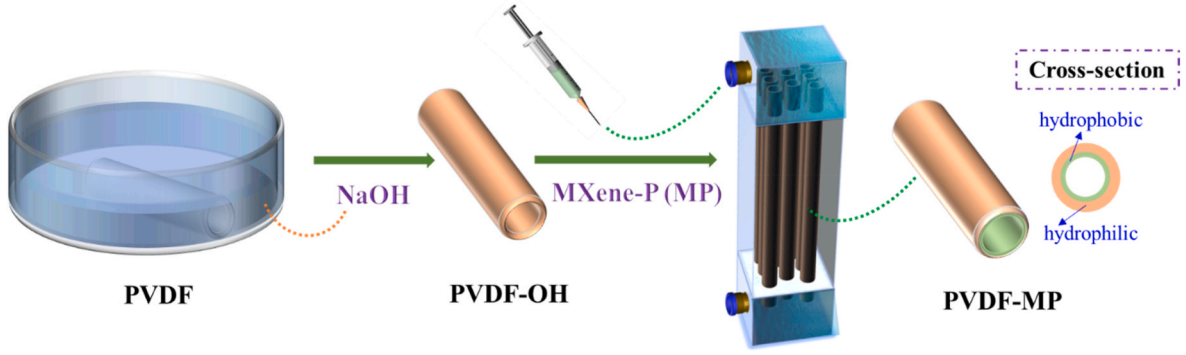

Fig. 1. Fabrication process for hydrophobically modified PVDF hollow fiber membranes.

insufficient for the water to nucleate on the surface of the membrane; thus, salts in the water cannot easily adhere to the membrane surface. Therefore, the successful preparation of a novel composite membrane with excellent hydrophobicity and durability has important practical applications.

Improving membrane hydrophobicity has been achieved through versatile techniques, such as blending, surface deposition, and chemical grafting [8,9]. Although current blending techniques are often easy to implement, the hydrophobic material cannot be fully exploited because of its tendency to become embedded inside the polymer instead of on the surface of the membrane. In addition, the distribution of hydrophobic material in the membrane is difficult to control, and its agglomeration may lead to serious performance degradation [13]. In the case of the surface deposition technique, the surface hydrophobicity of a membrane can be easily enhanced by coating a thin functional layer on its outer surface. The reliability and durability of the deposited layer are always unsatisfactory owing to the relatively weak interactions between the modified layer and substrate [7]. Surface chemical grafting can overcome these shortcomings by exposing most of the hydrophobic species to the outer membrane surface. In addition, chemical interactions between the substrate and functional materials make the surface durable. Thus, surface chemical grafting shows great potential for the superhydrophobic modification of PVDF hollow fiber membranes [14].

Many researchers have focused on hydrophobic modifications of hollow fiber membrane surfaces in membrane distillation fields [15,16], but mostly on outer surfaces. For MHDD, modification of the inner surface of the hollow fiber membrane is necessary, because salt water should flow inside the membrane fibers and air should flow outside to

Table 1
Orthogonal design for the synthesis of the PVDF-modified hollow fiber membranes based on five reaction factors and five treatment levels.

Factor level	A	B	C	D	E
	Immersion time in NaOH aq. (s)	Concentration of NaOH aq. (mol/L)	Contact time with MXene-P solution (h)	Reaction temperature with MXene-P solution (°C)	Reaction time with MXene-P solution (h)
1	5	1	1	40	0.5
2	10	2	3	60	1
3	30	4	5	80	2
4	60	6	7	100	3
5	120	8	9	120	4

minimize pressure drops. However, the intrinsic hydrophobicity of PVDF membranes (contact angle [CA], 110.3°) restricts the water solution used to modify the surface from entering the inner surfaces of the fine fibers. Furthermore, direct coating with a superhydrophobic solution is not feasible. In this study, PVDF hollow fiber membranes were first defluorinated so that the coating solution could enter and make full contact the inner surface (Fig. 1). Hydrophobic modification was then achieved via the interfacial dehydration reaction of the penetrated coating solution, and the detailed reaction mechanism was explained.

Moreover, the CA test method for hollow fiber membranes used by many researchers (typically by flattening the hollow fiber membrane) is similar to that used on flat membranes [9,17]. Nevertheless, the CA is related to surface curvature [18] and, crucially, the surface properties of flat and hollow fiber membranes are different. Thus, in this study, a new method for measuring the surface CA of a hollow fiber membrane that accounts for its degree of bending is proposed. When the curvature is considered in this way, the CAs of the inner and outer surfaces of the hollow fiber membrane differ from the corresponding planar CA [19].

Herein, a method for assembling 1H,1H,2H,2H-heptadecafluorodecyltrimethoxysilane (PFDTMS)-modified MXene (MXene-P) nanocomposite on the inner surfaces of a PVDF hollow fiber membrane is proposed using an interfacial reaction to enhance antiwetting and antifouling performance. Following this approach, a PVDF hollow fiber membrane is first defluorinated, creating hydrophilic properties via the creation of hydroxyl groups on its surface. Then, MXene-P is grafted onto the inner surface of the membrane through a hydrolysis reaction to improve hydrophobicity. Thus, a hydrophobic-hydrophilic MXene/PVDF composite hollow fiber membrane is successfully prepared and utilized in MHDD. In the composite membrane, PFDTMS reduces the membrane surface energy, MXene increases the surface roughness, and the hydrophilic substrate improves the water vapor transfer rate. Prepared membranes using this technique also exhibit excellent antiwetting and antifouling properties. In addition, a new technique for measuring the CAs of these modified membranes is described, and membrane durability is also evaluated under real seawater conditions. This work promotes the industrial application of hollow fiber membrane for desalination.

2. Materials and methods

2.1. Materials

MAX (Ti_3AlC_2) powders (particle size <38 μm, 400 mesh; purity >99 wt%) were purchased from Laizhou KaiKai Ceramic Materials

Table 2
Test case configuration and experimental results based on the orthogonal table (see Table 1).

Test case	Column					Contact angle (°)
	A	B	C	D	E	
	Immersion time in NaOH aq. (s)	Concentration of NaOH aq. (mol/L)	Contact time with MXene-P solution (h)	Reaction temperature with MXene-P solution (°C)	Reaction time with MXene-P solution (h)	
1	5	1	1	40	0.5	113.6
2	5	2	3	60	1	114.6
3	5	4	5	80	2	152
4	5	6	7	100	3	146.9
5	5	8	9	120	4	118.5
6	10	1	3	80	3	144.3
7	10	2	5	100	4	136
8	10	4	7	120	0.5	123.9
9	10	6	9	40	1	149.2
10	10	8	1	60	2	132.8
11	30	1	5	120	1	134.9
12	30	2	7	40	2	153
13	30	4	9	60	3	143.2
14	30	6	1	80	4	144.9
15	30	8	3	100	0.5	129.1
16	60	1	7	60	4	140.4
17	60	2	9	80	0.5	141.8
18	60	4	1	100	1	137.7
19	60	6	3	120	2	138
20	60	8	5	40	3	107.7
21	120	1	9	100	2	133.7
22	120	2	1	120	3	134
23	120	4	3	40	4	138
24	120	6	5	60	0.5	135.9
25	120	8	7	80	1	110
K_1	129.12	133.38	132.6	132.3	128.86	
K_2	137.24	135.88	132.8	133.38	129.28	
K_3	141.02	138.96	133.3	138.6	141.9	
K_4	133.12	142.98	134.84	136.68	135.22	
K_5						

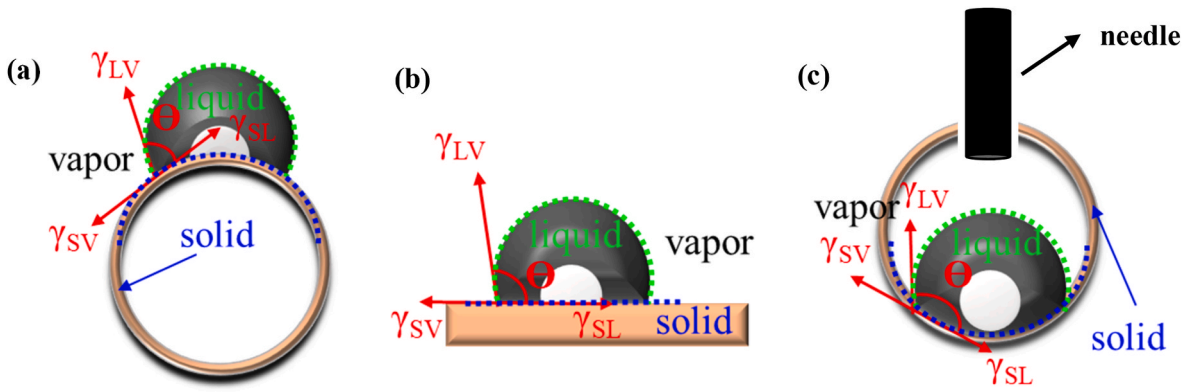

Fig. 2. Schematic diagram of the CAs of droplets on (a) PVDF outer surfaces (convex); (b) flat substrates; and (c) PVDF inner surfaces (concave). γ_{SV}, γ_{SL}, and γ_{LV} represent the surface tension coefficients of solid-gas, solid-liquid, and liquid-gas surfaces, respectively.

Table 3
Contact angles of the PVDF hollow fiber membranes.

Contact angle (°)	Traditional method	New method	Surface tension method [27]
PVDF outer surface	88.78 ± 3.0	78.68 ± 1.9	77.12 ± 3.3
PVDF inner surface	98.17 ± 2.1	110.3 ± 2.7	116.92 ± 2.4

Company Ltd. (Shandong, China). Acetic acid (CH_3COOH, 99.8%), PFDTMS, lithium fluoride (LiF, 99%), and polyethylene glycol (PEG, molecular weight 400) were obtained from Shanghai Aladdin Biochemical Technology (Shanghai, China). PVDF powder (molecular weight 500,000) was purchased from Dongguan De'an Plastic Company Ltd. (Guangdong, China). Hydrochloric acid (HCl, 37%), isopropyl alcohol (>99%), sodium hydroxide (NaOH, 99%), ethanol (99.5%), N, *N*-Dimethylacetamide (DMAC, 99.97%), and deionized water (DW) were obtained from Guangzhou Qianhui Co. (China). All chemicals were used as received without further treatment.

2.2. *Synthesis of the PVDF hollow fiber membrane*

The PVDF hollow fiber membrane was prepared by dry-wet phase transformation [20]. PVDF and PEG with molecular weights of 400 were dissolved in DMAC, and the mixture was stirred and dissolved at 65°C for 2 h to form a uniform casting solution. The solution was then held at this temperature for 96 h without mixing for degassing. At a flow rate of 20 mL/min and under a nitrogen pressure of 0.3 MPa, the polymer solution was filtered through a spinneret filter. At the same time, the core

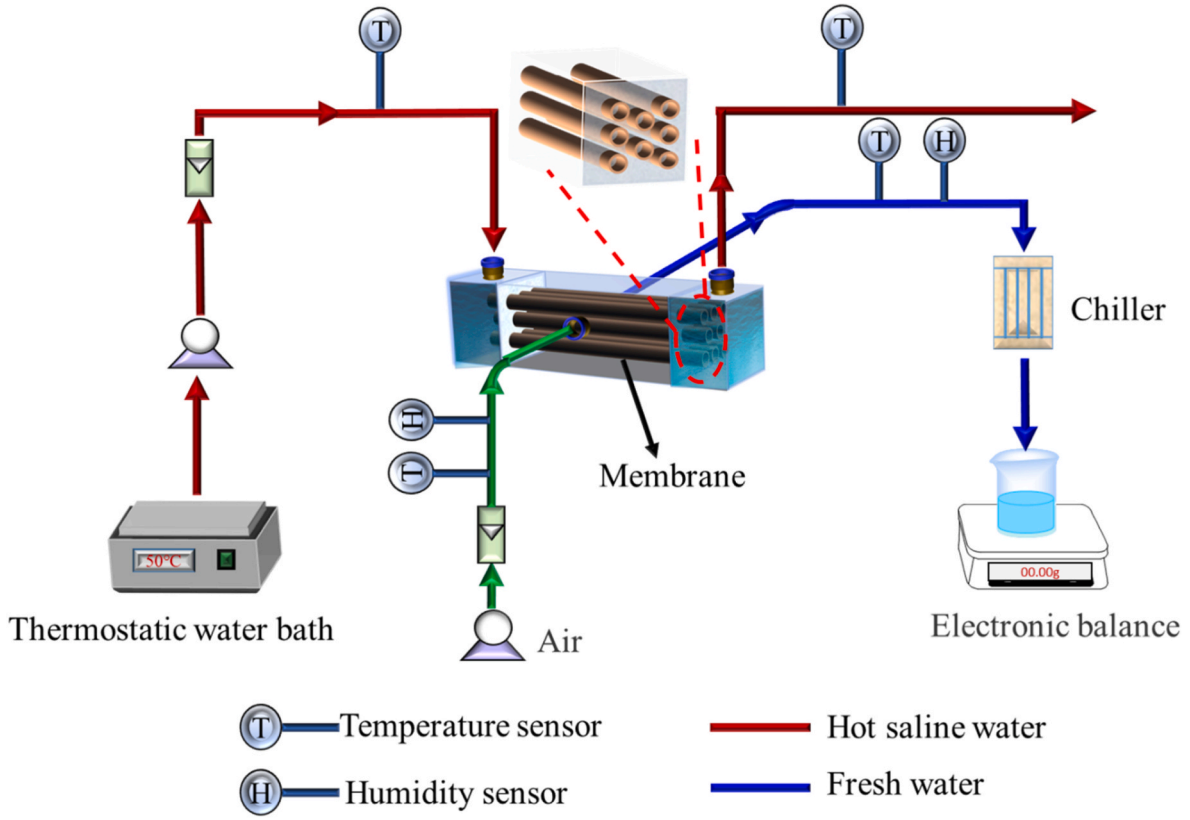

Fig. 3. Schematic diagram of measurements for hollow fiber membrane-based air humidification-dehumidification desalination.

Table 4
Physical and transport parameters of the hollow fiber module.

Symbol	Values	Unit	Symbol	Values	Unit
W	15	mm	D_{va}	2.49×10^{-5}	m^2/s
H	15	mm	D_{ws}	3.0×10^{-9}	m^2/s
L	80	mm	D_{vm}	9.11×10^{-7}	m^2/s
d_i	1.3	mm	$T_{a,i}$	20	°C
d_o	1.6	mm	$T_{s,i}$	50	°C
δ	0.15	mm	$\omega_{a,i}$	0.00927	kg/kg
P_D	2.5	mm	ω_s	0.0864	kg/kg
P_T	2.5	mm	ν_a	1.506×10^{-5}	m^2/s
P_L	2.17	mm	ν_s	5.56×10^{-7}	m^2/s
n_f	8	–	Sc_a	0.605	–
φ	9.1	%	Sc_s	185.3	–
A_v	227.56	m^2/m^3	Re_a	34.16	–
A_{tot}	0.0032	m^2	Re_s	734	–
ρ_a	1.205	kg/m^3	V_a	0.5	m^3/h
ρ_s	988.1	kg/m^3	V_s	200	mL/min

Table 5
Results of analysis of seawater from Yantian Coast, Shenzhen, southern China.

Parameter	Seawater	Parameter	Seawater
pH	9.0	Chlorine (mg/L)	16.62×10^3
Conductivity (mS/cm)	49.7	Fluorine (mg/L)	2.01
Turbidity	<1	Boron (mg/L)	2.65
Total organic carbon (ppm)	28.77	Calcium (mg/L)	362.04
Total inorganic carbon (ppm)	8.32	Potassium (mg/L)	330.05
Total plate count (CFU/mL)	6.1×10^3	Iron (mg/L)	0.058
$SUVA_{254}$ (L/mg m)	0.096	Sodium (mg/L)	9.68×10^3
UV_{254} (cm^{-1})	0.008	Magnesium (mg/L)	6.2×10^3
Humic acid (mg/L)	0.48	Manganese (mg/L)	<0.005
Amino acid (pmol/mL)	1154.60	Strontium (mg/L)	3.02

solution entered the inner cavity of the primary fiber at a flow rate of 35 mL/min from the central hole of the spinneret, was extruded into a coagulation bath at 40°C, and finally wound using a take-up winder. The spinneret temperature was maintained at 65°C in all experiments. The remaining solvent in the hollow fiber membrane was replaced by water by soaking the hollow fibers in a water bath for 96 h, and then allowed to dry naturally before use. The ambient temperature during the hollow fiber production process was approximately 20°C.

2.3. Synthesis of MXene-P (MP) solution

The MXene ($Ti_3C_2T_x$) solution was synthesized according to a previous study [21]. Briefly, 2 g of LiF was dissolved in 40 mL of 6 M HCl, and the mixed solution was stirred rapidly at room temperature for 5 min. Subsequently, 1 g of Ti_3AlC_2 was slowly added to the LiF/HCl mixture over a 5 min period to avoid bumping. The reaction was allowed to occur under continuous agitation at 35°C for 24 h. The resulting product was then washed with deionized water and centrifuged at 3500 rpm for 5 min. This process was repeated several times until the supernatant pH was >6. Then, the precipitate was dispersed in 100 mL of deionized water under ultrasonic conditions in a water bath for 30 min to delaminate the MXene flakes. Subsequently, the $Ti_3C_2T_x$ solution was centrifuged at 3500 rpm for 10 min. This process was repeated several times until no precipitate was observed in the centrifuge tube. The light-green supernatant, a colloidal solution of MXene, was then collected. To synthesize the MP solution, PFDTMS was reacted with MXene to modify the hydrophobic surface. The detailed procedure was as follows [22]: first, a hydrolytic solution of PFDTMS was prepared consisting of 0.5 vol% acetic acid, 2.0 vol% PFDTMS, and 97.5 vol% isopropanol [23]; second, the MXene aqueous solution and PFDTMS hydrolytic solution were mixed fully at a ratio of 10:5 (v/v) and ultrasonicated for 30 min at room temperature for further use.

2.4. Synthesis of the PVDF-modified hollow fiber membrane

To improve the interfacial force between the substrate membrane (PVDF) and modified solution (MP), the prepared PVDF hollow fiber membrane was first treated with NaOH solution, the product of which

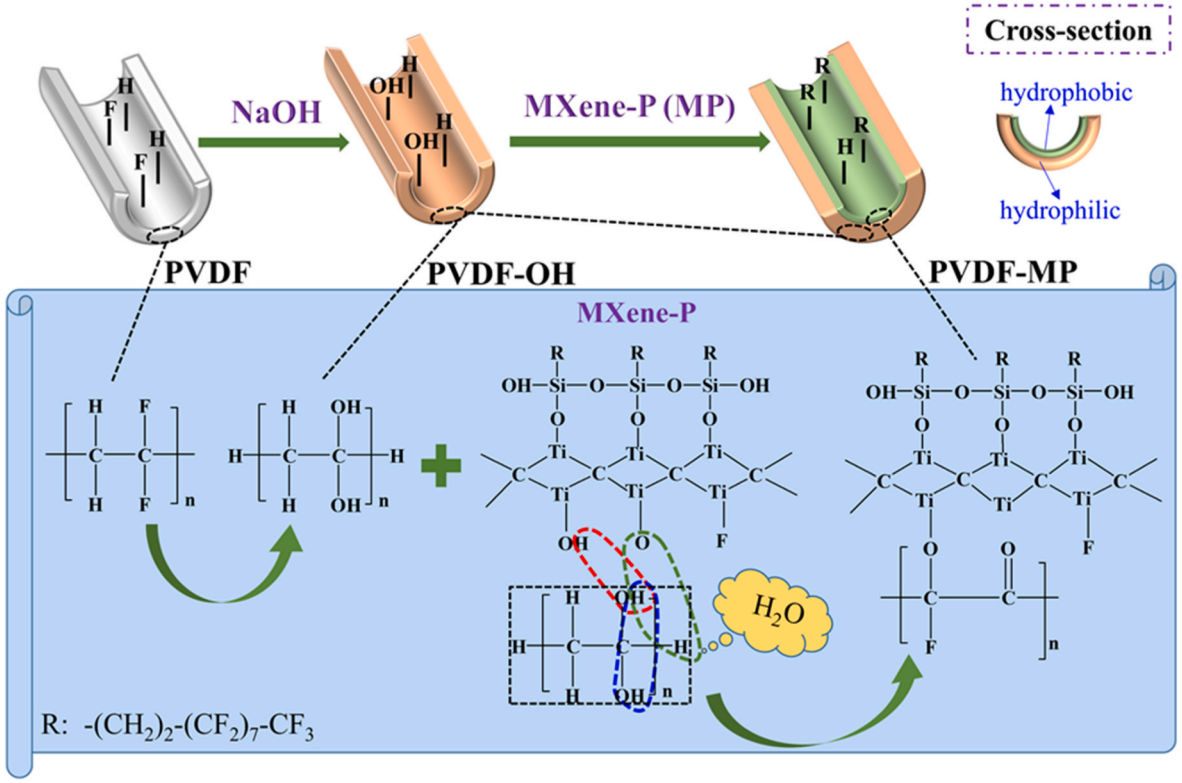

Fig. 4. Schematic diagram of the preparation and interfacial reaction mechanism for PVDF-MP hollow fiber membranes.

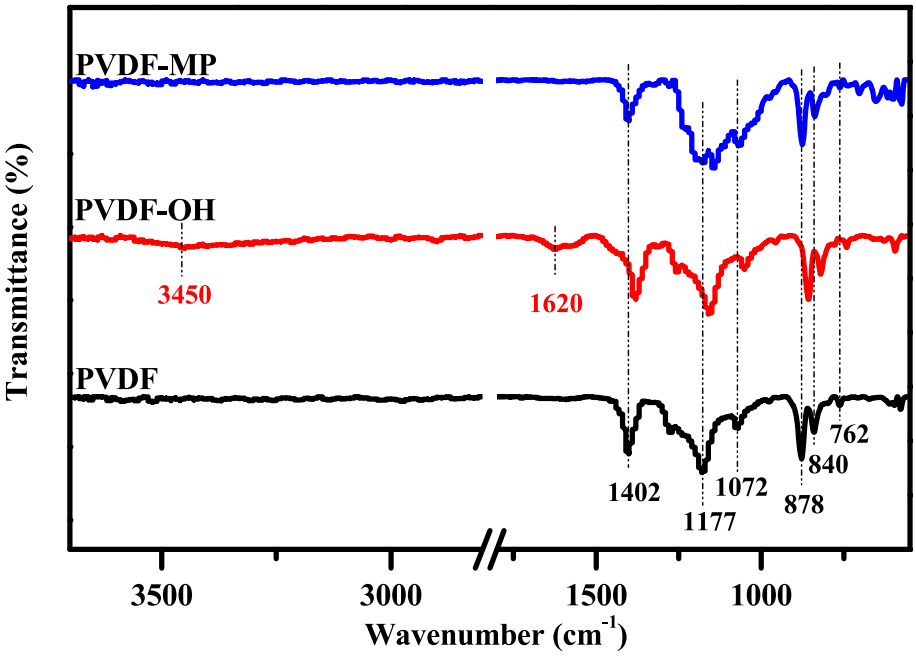

Fig. 5. ATR-FTIR spectroscopy of the PVDF, PVDF-OH, and PVDF-MP membranes.

was named as PVDF-OH. The MP solution was then passed within the PVDF-OH membrane to react with the hydroxyl groups on the PVDF-OH, producing the hydrophobic modification of the inner membrane wall. A schematic diagram of the fabrication process is shown in Fig. 1. As shown in Table 1, the influence of five factors on the reaction was considered (A, immersion time in the NaOH aqueous solution; B, the concentration of the NaOH aqueous solution; C, the contact time with the MP solution; D, the reaction temperature; and E, the reaction time with the MP solution), and 25 groups of orthogonal experiments were carried out. The CA results are shown in Table 2. K_i represents the average value of the CA corresponding to treatment level i under each factor (A–E), and R refers to range. According to the R values, A, B, and E had a greater influence on performance than C and D. For A, CA first increased and then decreased with immersion time in the NaOH aqueous solution, and the optimal condition was A3 based on the K_i value. The optimal conditions for the other four factors were B3, C5, D3, and E3, respectively. According to the CA values (Table 2), the optimal overall combination was A3/B4/C5/D3/E3.

The membrane modified under these optimal conditions was selected for subsequent testing using the following reaction steps: first, the 15-cm-long PVDF hollow fiber membrane was soaked in ethanol solution for 30 min, and the surface was wiped with filter paper to remove excess ethanol. Subsequently, after immersion in 6 mol/L NaOH for 30 s and reaction at 80°C for 2 h, the fluorine groups inside the PVDF membrane were partially replaced by hydroxyl groups. Second, a module was created with a bundle of the PVDF-OH membranes to form a shell-and-tube structure, and the module was placed vertically. MP solution was injected through the upper hole in the tube until it was full (the lower hole was sealed). The solution was kept full by replenishment as required, ensuring uniform deposition of MP on each fiber. After a 9-h reaction, the solution was emptied, and the tube was dried and dehydrated at 80°C for 2 h and 110°C for 2 h, respectively. The resulting hydrophobically modified membrane was named as PVDF-MP.

2.5. Characterization

The surface and cross-sectional morphological structures of the membranes were characterized by scanning electron microscopy (SEM, Merlin, Zeiss, Germany) together with energy-dispersive X-ray spectroscopy (EDXS) for the analysis of elemental composition and content. The samples were sprayed with gold before testing. The inner surface roughness of the membranes was also measured using atomic force microscopy (AFM, Multimode 8, Bruker, USA). Before observing the AFM image, small pieces of the membranes (1 × 1 cm) were cut and flattened on the sample table, and the non-destroyed portions were observed. A Nicolet IS50 spectrometer (Thermo Fisher Scientific, USA) was used to obtain attenuated total internal reflectance Fourier-transform infrared (ATR-FTIR) spectra of the membranes in the range 650–4000 cm^{-1}. X-ray photoelectron spectroscopy (XPS, Axis Ultra DLD, UK) was employed to obtain the elemental valence state at the membrane surface. Pore size distribution and tortuosity were measured using a mercury intrusion porosimeter (AutoPore9500, Micromeritics, USA). Finally, a thermal gravimetric analyzer (TG209F1, NETZSCH, Germany) was used to determine the thermal stability of the membranes in the 30–800°C range with a heating rate of 10 °C/min under an N_2 atmosphere.

2.5.1. Measurement of membrane porosity

Porosity was measured using the gravimetric method [24]. The dry membranes were first dehydrated overnight at 80°C before being weighed and then immersed in isopropanol for 2 h. The wet membrane weight was measured after the residual isopropanol on the membrane surface was removed. Three samples of each membrane were weighed and averaged. The membrane porosity was calculated as follows:

$$\varepsilon = \frac{(m_2 - m_1)/\rho_e}{(m_2 - m_1)/\rho_e + m_1/\rho_p} \quad (1)$$

where m_1 is the mass of the dry membrane (kg); m_2 is the mass of the wet membrane (kg); ρ_e is the isopropanol density (785.5 kg/m^3); and ρ_p is the polymer density (1190 kg/m^3).

2.5.2. Measurement of CA

The relative wettability of the membrane was determined by measuring the CAs of droplets on the membrane surface with a goniometer. CA is the angle between the line tangent to the wetted membrane surface and the droplet surface at the three-phase contact point [12]. The CA is related to the capillarity parameters of wetting problems using Young's equation [25], which describes the wetting properties of a

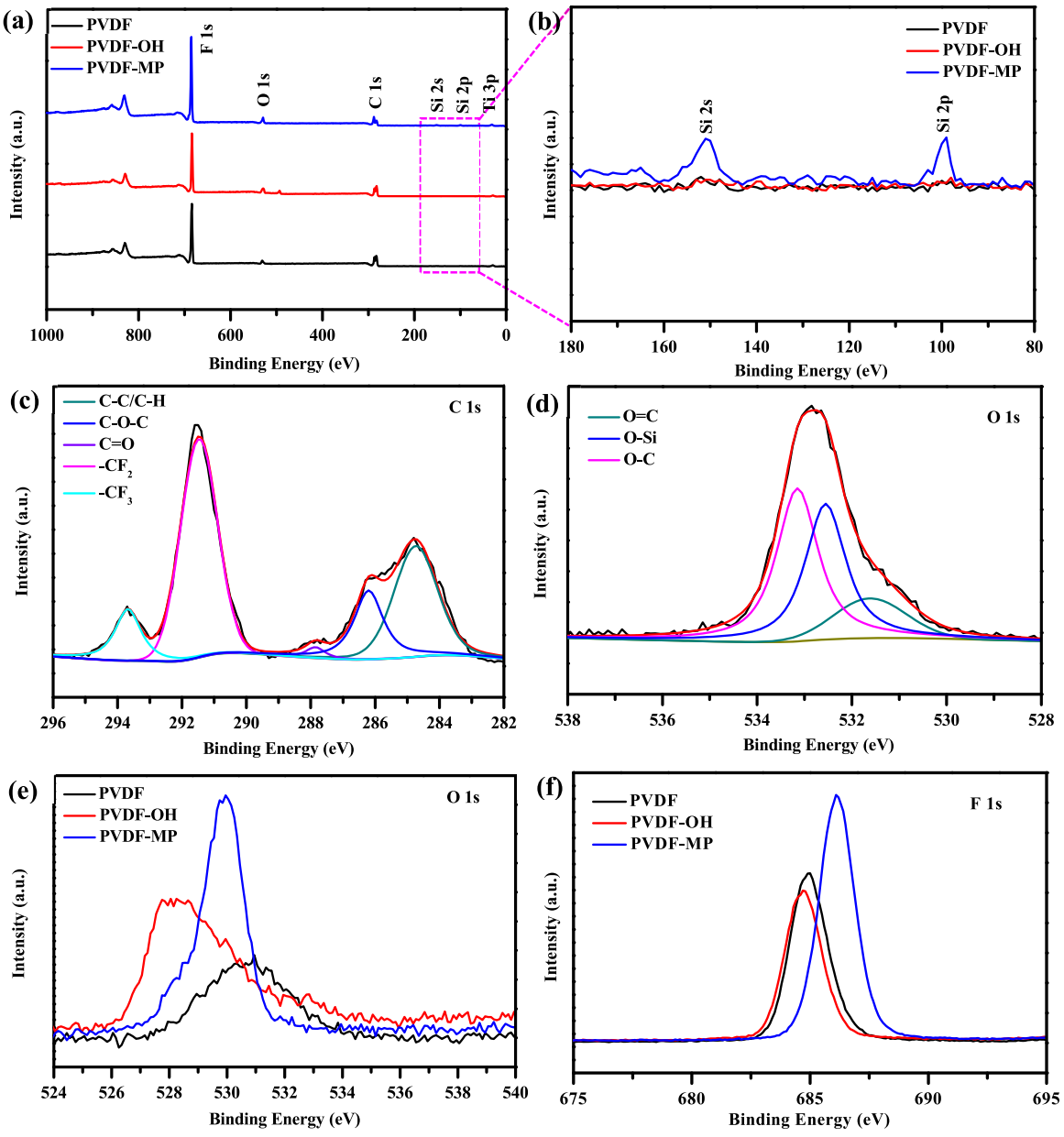

Fig. 6. XPS assessment of the PVDF membranes. (a) XPS spectra of the PVDF, PVDF-OH, and PVDF-MP hollow fiber membranes; (b) detailed spectra of the selected region in (a); (c) the C 1s scan spectra and (d) the O 1s scan spectra of the PVDF-MP hollow fiber membrane; (e) the O 1s scan spectra; and (f) the F 1s scan spectra of the PVDF, PVDF-OH, and PVDF-MP hollow fiber membranes.

Table 6
Element content (atomic %) from the XPS survey spectra of the three membranes.

droplet on a flat and smooth substrate. In reality, the surface of the PVDF hollow fiber membrane was rough and curved. Previous work [18,26] has also shown that CA values depend on the contact line curvature; however, the traditional method of measuring CA is to flatten the PVDF hollow fiber membrane prior to measurement, which does not reflect its working state. Therefore, a new method for measuring the CAs of hollow fiber membranes is proposed herein that considers the bending direction of the surface.

First, the membrane surface CAs were tested using an OCA40 Micro contact angle system (DataPhysics, Germany) with a 0.6 μL water droplet. For CA measurement on the outer surface (Fig. 2(a)), a droplet was placed on the outer membrane surface, and images were obtained by clicking the "Snap" button. The manual evaluation method of the system was used to determine the tangent formed by the droplet at the three-phase boundary where the liquid, gas, and solid intersected. The CAs were obtained by measuring the angle between the solid-liquid interface (γ_{SL}) and the gas-liquid interface (γ_{LV}) through the liquid interior. In contrast to the traditional method, a circular baseline (blue dotted line) was selected instead of a straight baseline (Fig. 2(b)). The CAs on the inner surface were measured following the same procedure, except that the top of the membrane was cut open to allow the water

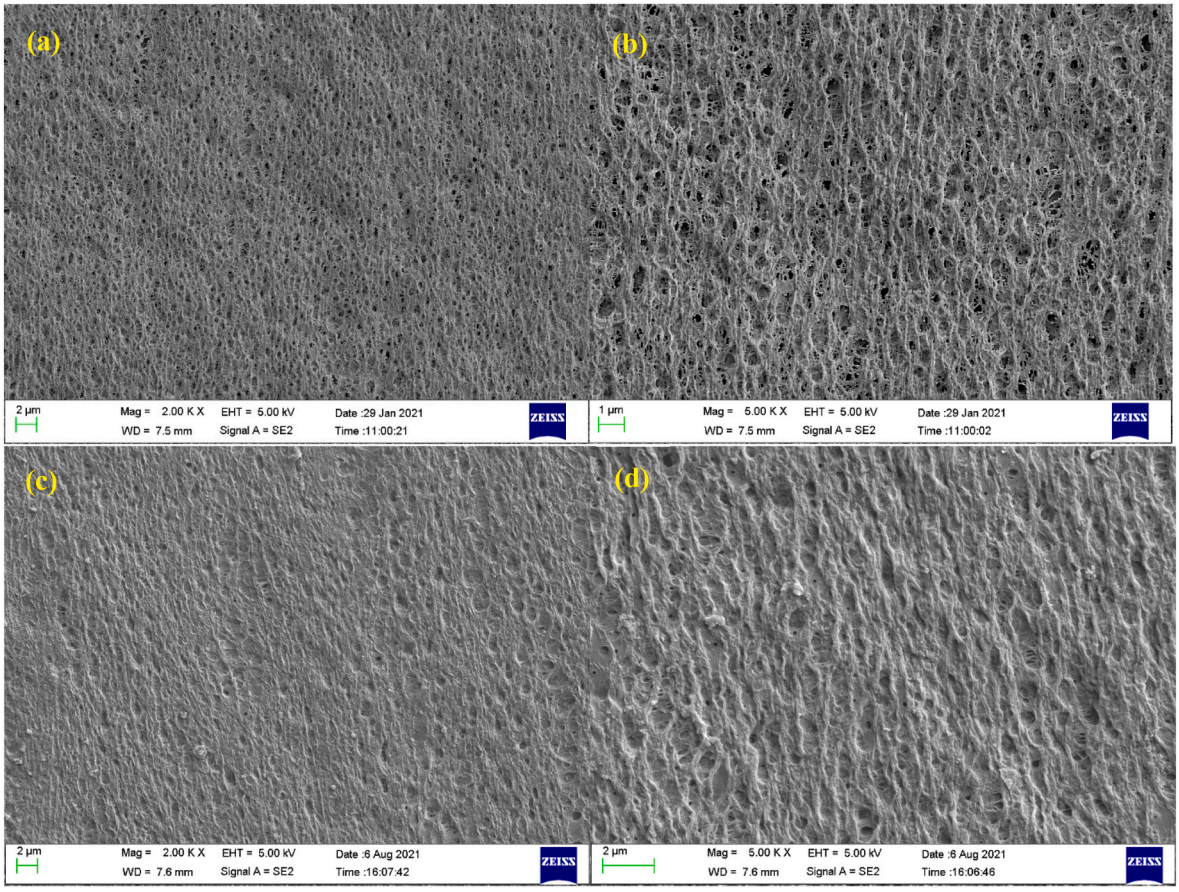

Fig. 7. Inner surface SEM images of the (a,b) PVDF and (c,d) PVDF-MP hollow fiber membranes at a magnification of (left) 2000 × and (right) 5000 × .

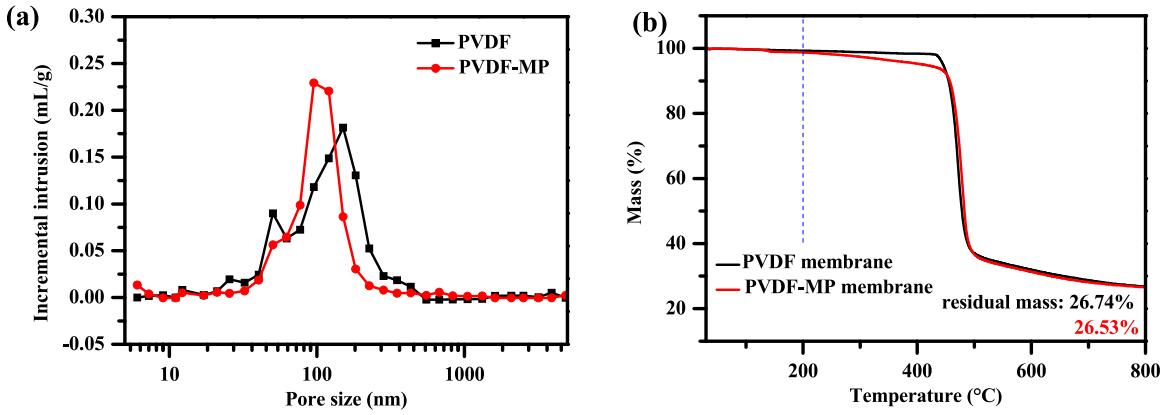

Fig. 8. (a) Aperture distribution of the PVDF and PVDF-MP hollow fiber membranes; (b) Thermogravimetric analysis of the PVDF and PVDF-MP hollow fiber membranes.

droplet to enter (Fig. 2(c)). The average CA of each sample was calculated at five different positions, and the values are listed in Table 3. The average PVDF outer surface CA measured using the traditional method was 88.78° compared to 78.68° using the new proposed method; for the PVDF inner surface, the corresponding values were 98.17° and 110.3°, respectively. Moreover, the CAs of the hollow fiber membrane were tested via surface tension effects based on previous reports [27] to verify the credibility of the method, the results of which are shown in Table 3. Compared to the traditional method (88.78° and 98.17°, respectively), the average CA of the hollow fiber membrane inner and outer surfaces using the new method (78.68° and 110.3°, respectively) were similar to those obtained by surface tension method (77.12° and 116.92°, respectively). Thus, a CA difference of 2% and 5.7% was detected for the outer and inner surfaces, respectively, between the new and surface tension methods. In comparison, differences of 13.1% and 16% were detected for the outer and inner surfaces between the traditional and surface tension methods. Thus, the proposed method is more intuitive, simple to implement, and convenient compared to the traditional method, and can be widely used to measure the CAs of hollow fiber membranes.

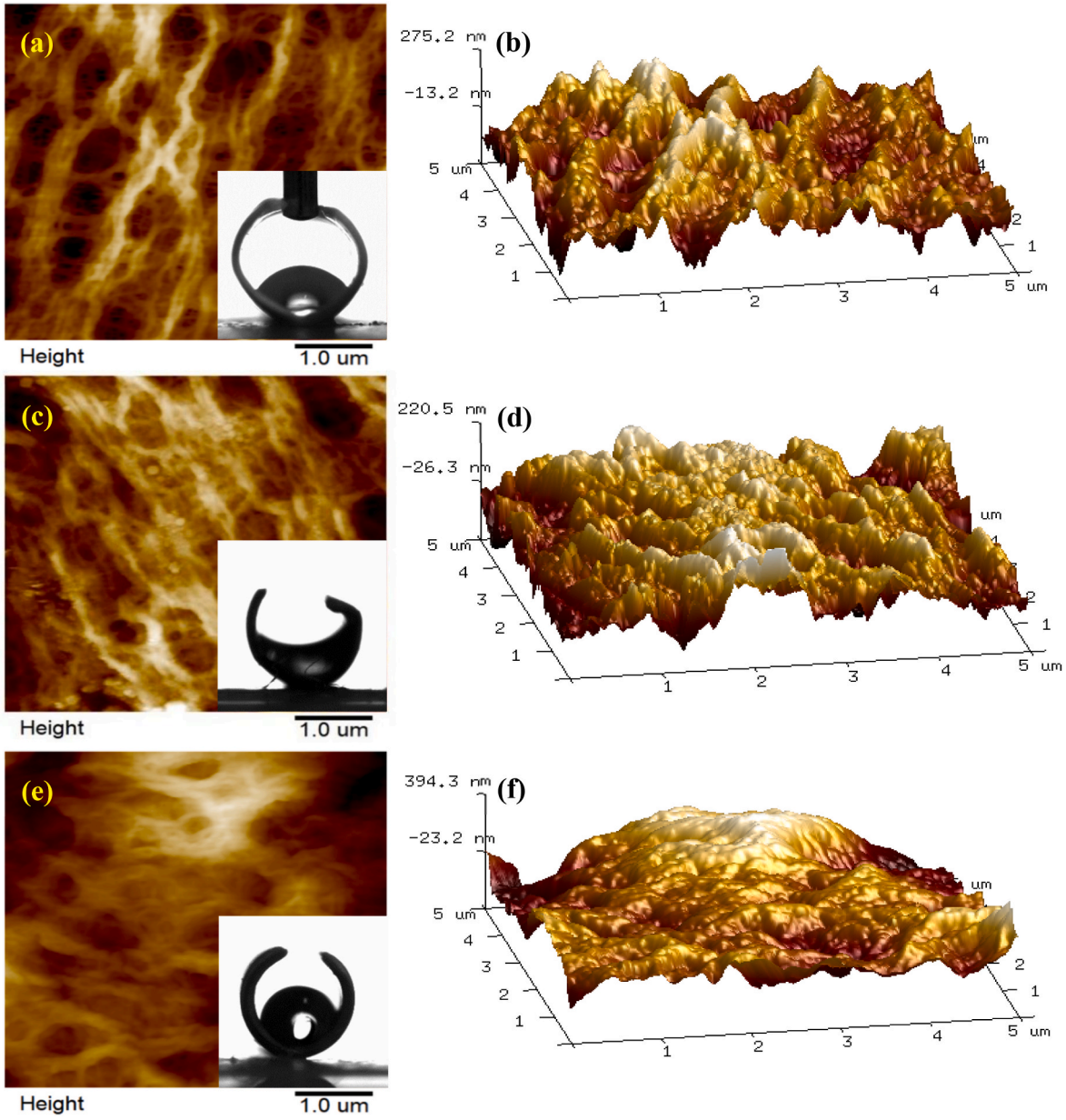

Fig. 9. AFM micrographs (scan size: 5 μm × 5 μm) of the PVDF (a,b), PVDF-OH (c,d), and PVDF-MP (e,f) inner surfaces: (left) top view and (right) 3D rendering. The inset image is the contact angle test diagram of the corresponding membrane.

Table 7
Roughness parameters of studied PVDF hollow fiber membranes.

Membrane	R_a (nm)	R_q

2.5.3. Calculation of the liquid entry pressure (LEP)

LEP_w is the initial pressure of the water entering the membrane pores, which was used to characterize the antiwetting ability of the membrane. LEP_w can be calculated using the Young–Laplace equation [7]:

$$\Delta P_{\text{Interface}} = P_f - P_p = \frac{-2\gamma_L B cos\theta}{r_{max}} \quad (2)$$

where P_p and P_f are the hydraulic pressures of the permeate and feed sides (Pa), respectively; γ_L is the liquid surface tension (72.84×10^{-3} N/m in this study); B is the geometric factor (assumed to be equal to 1 for cylindrical pores); θ is the CA; and r_{max} is the largest pore radius (m).

2.6. MHDD tests using seawater from the Yantian Coast

The MHDD system was comprised of a hollow fiber membrane module, condensation unit operation, and humidification unit. As shown in Fig. 3, the heated solution flowed within the fibers, and the air flowed across the fibers in a cross-flow manner. As the heated solution flowed within the membrane inner surface, moisture was transferred across the membrane, while the air was gradually humidified on the permeate side (the humidification process). Freshwater was then collected by condensing the humidified air via a cooler containing cold seawater (the condensation process). Eight fiber tubes in an equilateral triangular arrangement were assembled in the hollow fiber membrane module, providing an effective membrane area of 32 cm^2. Table 4 summarizes the physical and transport parameters of the hollow fiber

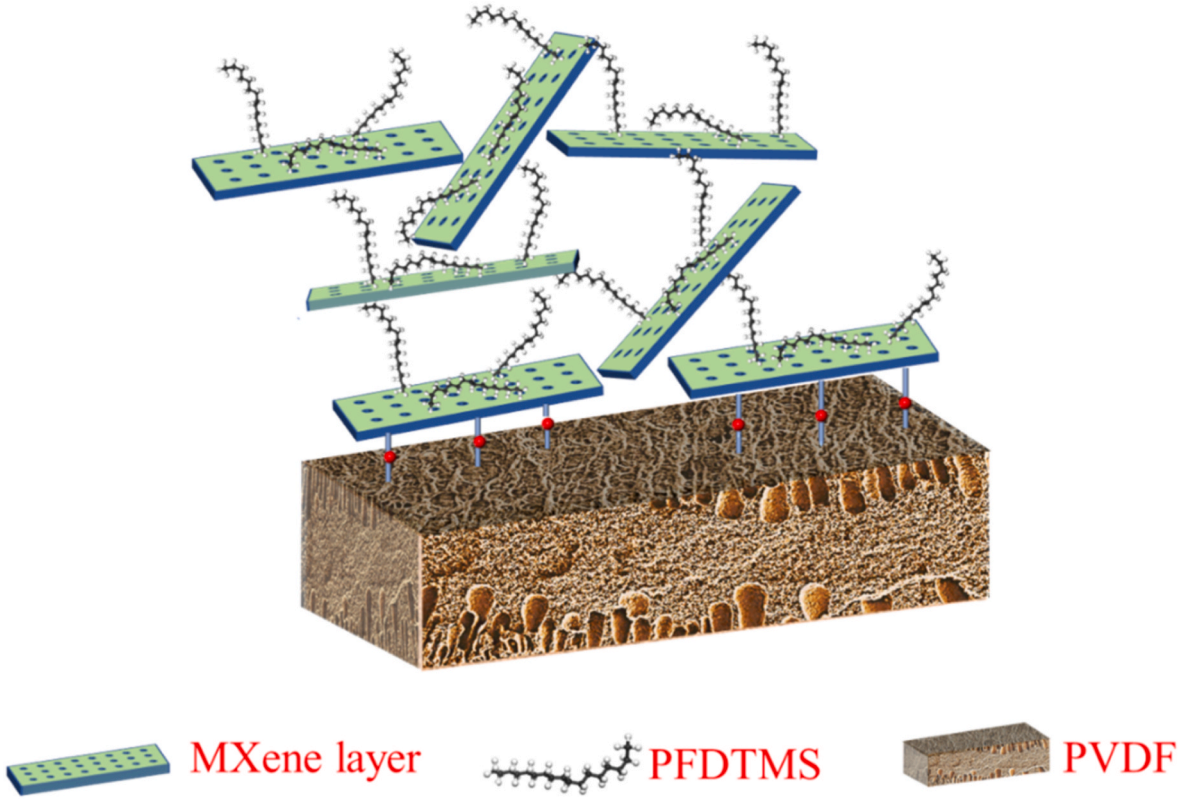

Fig. 10. Arrangement of MXene-P nanosheets on the PVDF substrate.

Table 8
Surface energies of studied PVDF hollow fiber membranes.

Membrane	WCA (°)	ECA (°)	Surface energy (mN/m)
PVDF	110.3	58.4	25.6
PVDF-OH	62.08	35.85	43.56
PVDF-MP	156.2	124	3.46

WCA, water contact angle; ECA, ethylene glycol contact angle.

Table 9
Parameters of water and ethylene glycol.

Liquid	SFT (total) (mN/m)	SFT (d) (mN/m)	SFT (p) (mN/m)
Water	72.8	21.8	51
Ethylene glycol	48.2	29.29	18.91

SFT, surface tension of the liquid; SFT (d), dispersive component of surface tension; SFT (p), polar component of surface tension.

module. System tests were conducted using seawater as the feed liquid. The flow rate was maintained at 200 mL/min, controlled by peristaltic pumps, and the temperature was set to 50°C using a thermostatic water bath. Seawater was collected from the Yantian Coast of Shenzhen, a coastal city in southern China; the composition of the seawater is shown in Table 5. Air was selected as the sweep gas on the shell side with a flow rate of 0.5 m^3/h and a temperature of 20°C. The temperature and humidity at the inlet and outlet were monitored in real-time using temperature and humidity sensors. All piping surfaces were covered with cotton insulation to prevent heat loss. The ambient relative humidity was ~60%. The permeate flux (J, kg/(m^2·h)) was calculated using Eq. (3) [28]:

$$J = \frac{m_a\left(\omega_{a,i} - \omega_{a,o}\right)}{A} \tag{3}$$

where m_a is the mass gain of air (kg/h); ω_a is the humidity of air (kg moisture/kg air); the subscripts i and o represent the inlet and outlet, respectively; and A is the effective area of the membrane (m^2).

The salt rejection rate (R, %) was calculated using Eq. (4) [29]:

$$R = \frac{C_f - C_p}{C_f} \times 100\% \tag{4}$$

where C_p and C_f are the salt concentrations of the permeate and feed solution (mg/L), respectively, which are positively associated with conductivity.

3. Results and discussion

3.1. Interfacial reaction mechanism of hydrophobic modification

The process and reaction mechanism of the hydrophobic treatment of the inner surface of the PVDF hollow fiber membrane are displayed in Fig. 4. The PVDF hollow fiber membrane was first treated with aqueous

Table 10
Pore size and liquid entry pressure of the PVDF and PVDF-MP hollow fiber membranes.

Membrane type	Porosity (%)	Tortuosity	Mean pore size (nm)	Largest pore size (nm)	Membrane thickness (μm)	Contact angle (°)	LEP_w

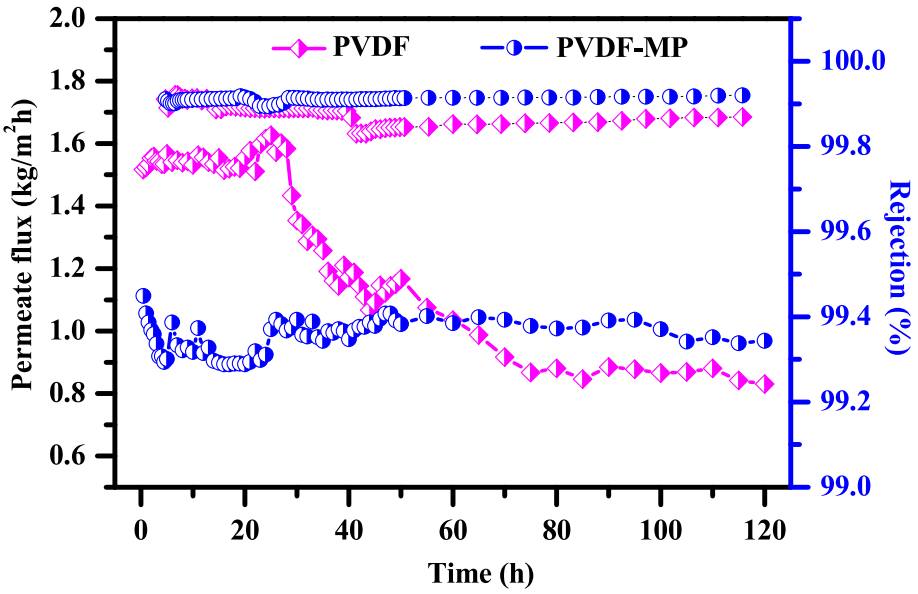

Fig. 11. Permeate flux and salt rejection rate of the membranes under actual seawater conditions.

NaOH solution, replacing the fluoride groups (-F) on inner surface with hydroxyl groups (-OH) and forming PVDF-OH [30]. Thus, the surface was converted from hydrophobic to hydrophilic. Then, the MP solution (PFDTMS-modified MXene) completely contacted the PVDF-OH surface, and a dehydration reaction occurred. Potential reactions are as follows: (1) as shown by the red dashed oval in Fig. 4, the H in MP and the OH in PVDF-OH were dehydrated to form C–O–Ti (C); (2) internal dehydration occurred in the PVDF-OH, forming C═O (blue dashed oval in Fig. 4); and (3) the water formed between an O in MP and 2H in PVDF-OH was removed, creating C═O (green dashed oval in Fig. 4). Thus, the interfacial force between the modified layer and substrate was enhanced. Moreover, the addition of PFDTMS decreased the surface energy, and the introduction of MXene increased the surface roughness, which made the inner surface superhydrophobic. Therefore, a hydrophobic-hydrophilic MXene/PVDF composite hollow fiber membrane was successfully realized.

3.2. *Structural characterization of the prepared hollow fiber membrane*

As shown in Fig. 5, ATR-FTIR spectroscopy confirmed the interfacial reaction mechanism. The PVDF membrane produced characteristic peaks at 1402 and 1177 cm^{-1} that were ascribed to C–F. Additional characteristic peaks were also observed including those at 1072, 878, and 762 cm^{-1} representing the α-phase crystal structure, and those at 840 cm^{-1} denoting the β-phase [31]. When treated with NaOH, the bands associated with C–F at 1402 and 1177 cm^{-1} were red-shifted, and new peaks at 3450 and 1620 cm^{-1} appeared that were ascribed to –OH. These findings confirm that the surface groups of the membrane were changed from C–F to C–OH. After modification with MP, the –OH peak disappeared. This verifies that MP reacted with the hydroxyl groups on the surface of the PVDF-OH. The peak shift could also be attributed to the existence of hydrogen bonding. The peaks in the 1000–1300 cm^{-1} spectral range attributed to the stretching bonds of Si–O–Si, C–O–C, and Ti–O–C were coincident with the characteristic peaks of the PVDF hollow fiber membrane. These findings support the reaction between MP and PVDF-OH described in Fig. 4.

The XPS spectra of the PVDF, PVDF-OH, and PVDF-MP hollow fiber membranes were determined to examine their chemical properties, as shown in Fig. 6. All membranes contained the C 1s, O 1s, and F 1s peaks typical of PVDF (Fig. 6(a)). Compared to the original PVDF membrane, the PVDF-MP membrane showed extra peaks corresponding to Si 2s (binding energy, 151.0 eV) and Si 2p (binding energy, 99.0 eV), as shown in Fig. 6(b). In particular, the surface fluorine content first decreased from 41.35% in PVDF to 39.39% in the case of the PVDF-OH membrane due to the change in partial surface groups from fluorine to hydroxyl, and then increased significantly to 53.98% when MP was grafted onto its surface (Table 6). The increased fluorine content was mainly due to the fluorine groups in MP. In addition, high-resolution C 1s and O 1s XPS spectra of the PVDF-MP membranes were obtained to characterize the chemical bonds. Based on Fig. 6(c), C 1s can be deconvoluted into five peaks matched to C–C/C–H, C–O–C, C═O, CF_2, and CF_3 with corresponding binding energies of 284.7, 286.2, 287.9, 291.5, and 293.7 eV [32], respectively. In the O 1s core level scan spectra (Fig. 6(d)), the three fitted peaks located at the binding energies of 531.6, 532.5, and 533.1 eV can be ascribed to O═C, O–Si, and O–C [33,34], respectively. In addition, compared to those in the PVDF and PVDF-OH membranes, the peak position and intensity of O 1s and F 1s both changed in the PVDF-MP membrane (Fig. 6(e and f)), which further confirms the interface interaction between the subject membrane (PVDF) and the modified solution (MP). These results provide further evidence of the interfacial reaction mechanism (Fig. 4).

3.3. *Morphology of the prepared hollow fiber membranes*

The surface morphologies of the pristine PVDF and PVDF-MP hollow fiber membranes are shown in Fig. 7. Highly porous structures were observed in the pristine PVDF membrane (Fig. 7(a)); however, the SEM images of the PVDF-MP membrane indicate that its surface was covered with MP (Fig. 7(c and d)). The EDX analysis results also support this conclusion (Fig. S1). Only the elements C and F were observed on the surfaces of the PVDF membrane (Fig. S1 (A1–4)), while O, Ti, and Si were uniformly spread on the surface of the PVDF-MP membrane. Ti was derived from MXene, and Si and O were derived from PFDTMS. Correspondingly, the mean pore size was reduced from 169.8 nm for the unadorned PVDF membrane to 161.6 nm for the PVDF-MP membrane after MP grafting (Fig. 8(a)). The aperture distribution of the PVDF-MP membrane was more uniform than that of the PVDF membrane.

Thermogravimetric analysis was also used to determine the thermal stability of the PVDF and PVDF-MP hollow fiber membranes, as shown in Fig. 8(b). Both membranes showed almost no loss of mass at temperatures below 200°C, which was much higher than our operation temperature of 60°C. This indicated that both membranes were thermally stable during the seawater treatment. Furthermore, a similar trend of weight loss in both membranes was exhibited at temperatures above

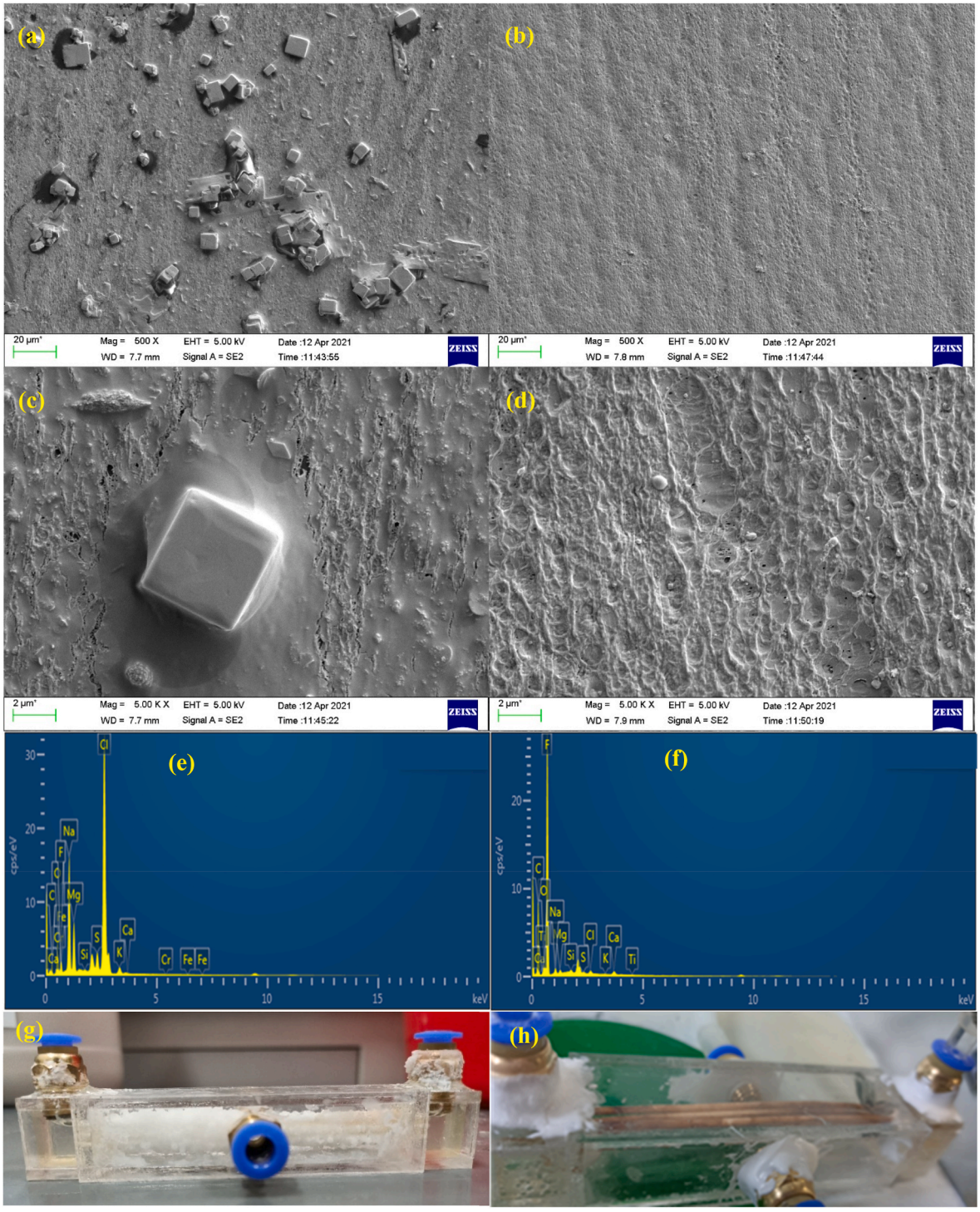

Fig. 12. Inner surface SEM images (a–d) and EDXS analyses (e,f) of the PVDF (left) and PVDF-MP (right) hollow fiber membranes after testing at different magnifications of (a,b) 500× and (c,d) 5000 × . Photographs of the PVDF (g) and PVDF-MP (h) membranes after the MHDD test.

436°C, and the residual mass was 26.74% for the PVDF membrane and 26.53% for PVDF-MP hollow fiber membrane. These results show that the degradation rate of the modified membrane was similar to that of the pure PVDF membrane. However, the mass change of the two membranes showed some differences between 200 and 436°C. Notably, the decomposition of the modified layer containing low-boiling point PFDTMS and abundant oxygen-containing functional groups may explain these results. Furthermore, these findings add to the evidence supporting the deposition of the modified layer on the membranes.

The roughness of a membrane surface plays a significant role in fouling resistance. The AFM graphs of the PVDF, PVDF-OH, and PVDF-MP hollow fiber membranes are shown in Fig. 9, and the arithmetic mean deviation (R_a) and mean square deviation (R_q) are listed in Table 7. Compared to that of the pristine membrane, the membrane roughness slightly decreased after replacing the fluorine groups with –OH. Correspondingly, the CA decreased from 110.3° to 62.08°. However, the roughness increased when MP was grafted on the surface, with the CA reaching 156°. This may reflect the irregular stacking of lamellar MP increasing the roughness of the PVDF-MP membrane surface. A possible arrangement of the MP nanosheets on the PVDF substrate is

Table 11
Elemental composition of contaminants on the hollow fiber membrane surfaces after testing.

Element content (wt%)	PVDF	PVDF-MP
C	20.77	36.66
O	17.58	3.32
F	5.42	56.81
Na	15.16	1.17
Mg	6.34	0.48
Si	0.14	0.27
S	2.37	0.24
Cl	30.82	0.38
K	1.27	0.03
Ca	0.04	0.59
Fe	0.09	0.00
Ti	0.00	0.04

shown in Fig. 10. When water contacts the rough surfaces, air is trapped in the micro/nano structures of the surfaces forming the Cassie state [35], which reduces the contact area between the drop and membrane surface, and results in superhydrophobicity.

In addition to roughness, low surface energy is an important factor affecting the durability of membranes during seawater treatment. Thus, the surface energy of the membranes was calculated using the CA of two test liquids on each solid surface based on Neumann's equation of state [36], as shown in Table 8. The two test liquids were water and ethylene glycol, and their parameters are listed in Table 9. The calculated surface energy of PVDF was 25.6 mN/m, similar to what has been reported in the literature (i.e., 30.3 mN/m [1]); minor differences may be due to the different preparation conditions. The surface energy of the PVDF-OH membrane was 43.56 mN/m, which was 70% higher than that of the original PVDF hollow fiber membrane due to the presence of –OH groups. Notably, MP played a key role in reducing the surface energy because of its close interaction with the PVDF-OH surface hydroxyl groups. The surface energy of PVDF-MP was reduced by 86.5% and 92% compared to the pristine PVDF and PVDF-OH membranes, respectively. Many fluorine groups on the PVDF-MP surface may have contributed to this observation. Membranes with a high CA (high hydrophobicity), small pore size, and low surface energy possess high liquid entry pressures (LEP_w) [37]. The LEP_w values of the PVDF and PVDF-MP hollow fiber membranes are listed in Table 10. The tested LEP_w was 182.36 kPa for the PVDF hollow fiber membrane and 392.97 kPa for the PVDF-MP membrane, which represents a 1.15-fold increase compared to the pure membrane. The high LEP_w for the PVDF-MP membrane means that seawater could not easily penetrate the membrane pores, resulting in excellent membrane durability.

3.4. *Fouling resistance tests*

The PVDF and PVDF-MP hollow fiber membranes were tested with MHDD under real desalination conditions to verify their durability when subjected to 120 h of continuous seawater treatment (Fig. 11). The salt rejection rate of both membranes remained largely constant over the entire operation period at >99.8%. The salt rejection rate of the PVDF-MP membrane was superior to that of the pristine PVDF membrane after 40 h due to its excellent antifouling ability. The permeate flux of the PVDF hollow fiber membrane began to decrease steadily from 1.5 to 0.8 kg/(m^2·h) after treating seawater for 28 h. Salt crystals were observed on the outer surface of the fiber membrane, as shown in Fig. 12(g), indicating wetting on the inner surface. The low LEP_w and visible contaminants on the inner surface of the PVDF membrane (Fig. 12(a,c)) may explain this phenomenon. The contaminants mainly consisted of salt crystals (e.g., NaCl and KCl) and limescale (e.g., $MgSO_4$ and $MgCO_3$), as determined using EDXS (Fig. 12(e), Fig. S2, and Table 11). The contaminants attached to the inner surface increased the surface energy and mass transfer resistance of the membrane, prompting membrane wetting and, thus, reducing the flux.

In contrast, the permeate flux of the PVDF-MP membrane was lower than that of the original PVDF membrane. This was because an extra layer of MP had coated the PVDF surface, resulting in an increase in mass transfer resistance. The hydrophobic-hydrophilic composite membrane also increased the vapor permeation rates [38]. The opposing effects of these two properties jointly determined the flux of the PVDF-MP membrane. The PVDF-MP membrane performance was stable during the desalination process, at approximately 1.0 kg/(m^2·h) with slight fluctuations (Fig. 11); no salt crystals were visible on its outer surface (Fig. 12(h)), indicating excellent durability and antiwetting ability. In addition, few contaminants were visible on the inner surface of the membrane, as shown in Fig. 12(b) and (d).

The surface composition of the membranes was further analyzed by EDXS (Fig. 12(f) and Fig. S3), as summarized in Table 11. The fluorine

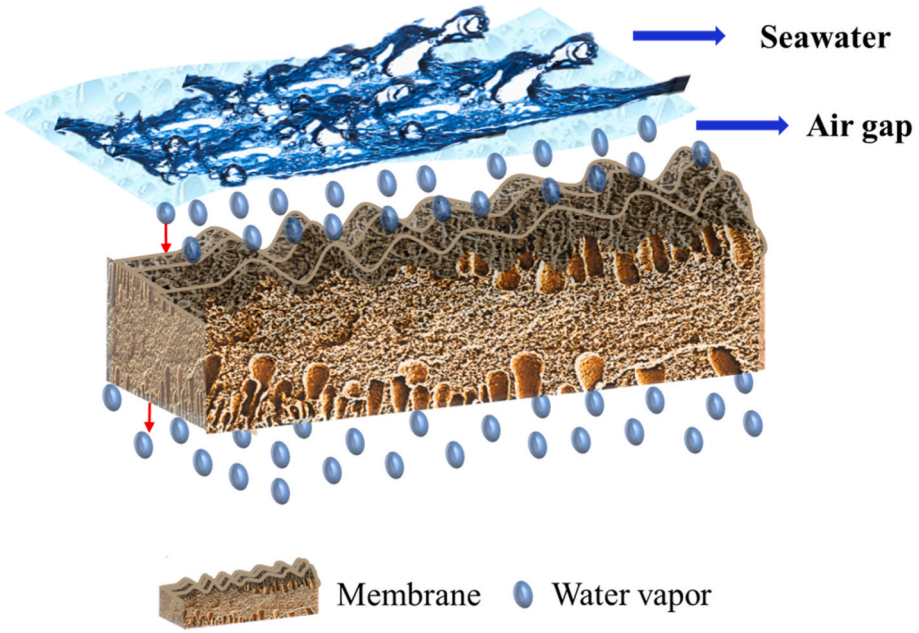

Fig. 13. Antifouling mechanism of the PVDF-MP hollow fiber membrane.

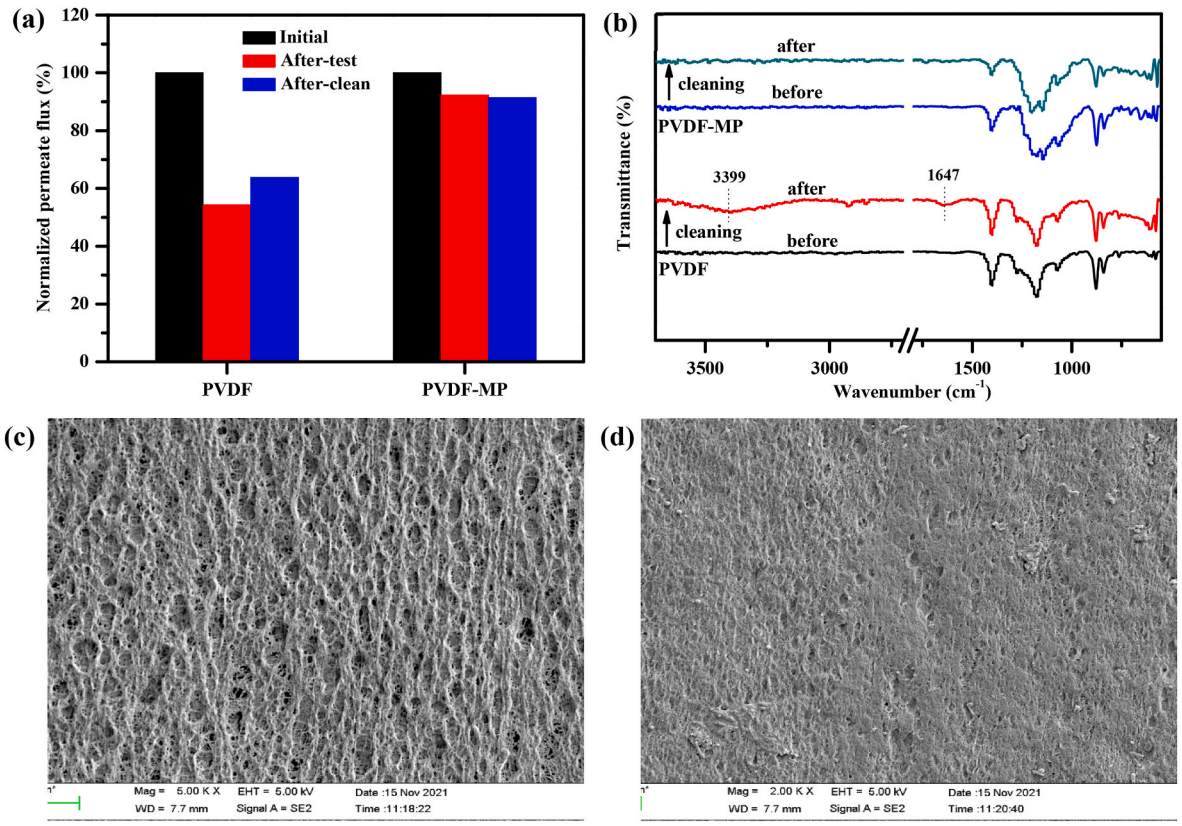

Fig. 14. (a) Normalized membrane permeate flux of the PVDF and PVDF-MP hollow fiber membranes after 120-h testing and after chemical cleaning. (b) FTIR spectra of the PVDF and PVDF-MP membranes after chemical cleaning. SEM images of the PVDF (c) and PVDF-MP (d) hollow fiber membranes after cleaning with citric acid.

Table 12
Mass transfer coefficients of the PVDF and PVDF-MP hollow fiber membranes.

Membrane type	δ_m (μm)	J (kg/(m^2 h))	k_{tot} (× 10^{-3} m/s)	k_a (× 10^{-2} m/s)	k_s^e (× 10^{-1} m/s)	k_m (× 10^{-3} m/s)	k_{m1} (× 10^{-3} m/s)	k_{m2} (× 10^{-2}

content of the PVDF-MP membrane was higher than that of the PVDF membrane due to the addition of the fluorine groups from MP, which is consistent with the XPS results (Table 6). The contents of other elements were lower than those of the PVDF membrane, demonstrating less surface contamination. There are two possible explanations for the excellent wetting resistance and fouling resistance of the PVDF-MP membrane. On the one hand, owing to its rough surface structure (Table 7 and Fig. 13), air gaps could form between the PVDF-MP membrane surface and seawater, which may prevent contaminant deposition and, thereby, improve the antifouling ability [30]. On the other hand, LEP_w was increased (Table 10) owing to the low surface energy of the membrane (Table 8), hampering seawater penetration into the membrane pores and improving its antiwetting ability.

Chemical cleaning was also performed to further demonstrate the durability of the membranes. The cleaning procedure was performed as follows: first, deionized water was flowed through the inner surface of the membranes at 200 mL/min for 30 min; then, 0.1 wt% citric acid was used for cleaning for 20 min; finally, the remaining acid on the membrane inner surfaces was washed with deionized water for 30 min. The normalized permeate fluxes of the PVDF and PVDF-MP hollow fiber membranes after 120-h testing and chemical cleaning are shown in Fig. 14(a). After 120 h, the flux of the pure PVDF membrane was attenuated to 54.3% of the initial flux compared to 92.3% for the modified PVDF membrane, which was within its normal fluctuation range. After cleaning, the flux of the original membrane recovered to 63.84% of the initial flux compared to 91.41% for the modified membrane. Changes in the surface functional groups were also analyzed by comparing the FTIR spectra between the chemically cleaned and the initial membranes (Fig. 14(b)). The spectra of the cleaned membranes were in accordance with the corresponding initial membranes, except for peaks at 3399 and 1647 cm^{-1} in the PVDF membrane after cleaning, which were ascribed to the –OH of the water. Predictably, no change in the membrane structure was observed after the use of citric acid. In addition, according to the SEM results, the surface morphologies of the PVDF and PVDF-MP membranes were not damaged after chemical cleaning with citric acid (Fig. 14(c–d)). Most notably, a smaller reduction in the permeate flux of the PVDF-MP membrane was observed after the test compared to the PVDF membrane. This is attributed to the superhydrophobic coating on the modified membrane, which likely prevented the adhesion of contaminants and the structure of which was not damaged by the citric acid treatment. Thus, the durability and the antifouling ability of the modified membrane were better than those of the pure PVDF membrane.

3.5. Calculation of mass transfer coefficients

The permeate flux of the studied membranes was influenced by several factors including flow conditions, flow manner, packing fraction,

and fiber arrangement. Therefore, the mass transfer coefficient (Table 12), which reflects the intrinsic properties of a membrane, was calculated by considering the resistance of both fluid sides. Here, the Reynolds number (*Re*) of both fluid sides was substantially less than 2300; thus, the flow is considered laminar. The thickness of the PVDF and PVDF-MP membranes (δ_m) was measured using a micrometer, and the permeate flux (kg/m^2·h) was measured using the MHDD setup. The total mass transfer coefficient (k_{tot}) was calculated using Eqs. S(1)–(7), yielding values of 4.67×10^{-3} and 3.43×10^{-3} m/s for the PVDF and PVDF-MP membranes, respectively. The equivalent mass transfer coefficient on the seawater side (k_s^e) was 0.547 m/s based on Eqs. S(9)–(15), and the air-side mass transfer coefficient (k_a) was 3.33×10^{-2} m/s based on Eqs. S(16)–(22). Thus using Eqs. S23 and S24), the mass transfer coefficients (k_m) of the PVDF and PVDF-MP hollow fiber membranes were found to be consistent with the reported literature [28]. Specifically, the mass transfer coefficient of the first substrate layer of the PVDF-MP membrane was 6.07×10^{-3} m/s, and that of the second hydrophobic layer was 1.42×10^{-2} m/s, which is one order of magnitude larger than that of the first layer. Therefore, the main mass transfer resistance of the modified membrane is a function of the substrate layer thickness. Based on this finding, thinner support layers should be used in future if adequate mechanical strength can be maintained.

4. Conclusions

PVDF hollow fiber membranes are considered more suitable for industrial humidification-dehumidification seawater desalination because of their easy processing and high packing-density properties. However, the disadvantages of scaling and wetting of their inner surfaces hinder sustainable application. Improving the superhydrophobicity of the inner surfaces of these membranes is regarded as an effective way to overcome these challenges, yet achieving contact between the coating solutions the interior surfaces of PVDF membranes has provided difficult because of their inherent hydrophobic properties. Consequently, relative to those focusing on outer surfaces, few studies have successfully demonstrated the hydrophobic modification of the inner surfaces of membranes.

Here, PVDF membrane was first defluorinated (PVDF-OH), changing its surface from hydrophobic to hydrophilic. Then, the coating solution (MP) was injected into the membrane fibers to achieve full contact with the inner surfaces. Superhydrophobicity of the inner surface was subsequently realized via an interfacial dehydration reaction. The final prepared membrane had an inner surface CA of 156.2°, which was determined using a novel technique that accounts for surface curvature. The surface energy and roughness modifications resulting from the described treatment explain the observed differences in membrane characteristics; PFDTMS reduced the surface energy, and the layered structure of MXene increased roughness. Thus, a hydrophobic-hydrophilic MXene/PVDF composite hollow fiber membrane was successfully fabricated and utilized in an MHDD system to evaluate its long-term seawater treatment performance. The PVDF-MP hollow fiber membrane exhibited excellent durability and stable permeate flux rates during a 120-h continuous seawater desalination test. In addition, no fouling or wetting occurred during the entire procedure. In contrast, for conventional PVDF hollow fiber membranes, the permeate flux rate began to decrease steadily after 28 h, and wetting and fouling were also observed. High LEP_w values prevented water from permeating the modified membranes, thereby producing antiwetting properties. Furthermore, the air gaps formed between the superhydrophobic surface and seawater hindered the deposition of contaminants, enhancing the membrane's antifouling properties. Overall, the superior properties and performance of the described MXene/PVDF composite membranes in this study provides a sustainable roadmap for the widespread use of hollow fiber membrane-based MHDD systems.

Author contribution

Zhang Tao conducted the experiments and wrote the manuscript. Investigation, Guo Xin prepared PVDF hollow fiber membrane. Assistance, B. Solomon helped the analysis. Analysis, M. Sharifpur helped the writing. Writing, Zhang Li-Zhi concepted the study and supervised the project. Conceptualization.

Declaration of competing interest

The authors declare that they have no known competing financial interests or personal relationships that could have appeared to influence the work reported in this paper.

Acknowledgments

This project was supported by Natural Science Foundation of China (No. 51936005), and the National Key Research and Development Program of China (No. 2017YFE0116100). This work was also supported by the Key Project of Science and Technology Program of Guangzhou, China (No. 201904020027). The manuscript was edited for English language, grammar, punctuation, spelling, and overall style by Wiley Editing Services.

Appendix A. Supplementary data

Supplementary data to this article can be found online at https://doi.org/10.1016/j.memsci.2021.120146.

References

[1] A. Alkhudhiri, N. Darwish, N. Hilal, Membrane distillation: a comprehensive review, Desalination 287 (2012) 2–18.
[2] G.P. Li, L.Z. Zhang, Conjugate heat and mass transfer in a cross-flow hollow fiber membrane bundle used for seawater desalination considering air side turbulence, J. Membr. Sci. 533 (2017) 321–335.
[3] S.S. Ibrahim, Q.F. Alsalhy, Modeling and simulation for direct contact membrane distillation in hollow fiber modules, AlChE J. 59 (2013) 589–603.
[4] S. Meng, Y. Ye, J. Mansouri, V. Chen, Fouling and crystallisation behaviour of superhydrophobic nano-composite PVDF membranes in direct contact membrane distillation, J. Membr. Sci. 463 (2014) 102–112.
[5] Y.Z. Tan, H. Wang, L. Han, M.B. Tanis-Kanbur, M.V. Pranav, J.W. Chew, Photothermal-enhanced and fouling-resistant membrane for solar-assisted membrane distillation, J. Membr. Sci. 565 (2018) 254–265.
[6] D.Y. Hou, J. Wang, X.C. Sun, Z.G. Ji, Z.K. Luan, Preparation and properties of PVDF composite hollow fiber membranes for desalination through direct contact membrane distillation, J. Membr. Sci. 405 (2012) 185–200.
[7] M.K. Alsebaeai, A.L. Ahmad, Membrane distillation: progress in the improvement of dedicated membranes for enhanced hydrophobicity and desalination performance, J. Ind. Eng. Chem. 86 (2020) 13–34.
[8] H.B. Li, H.J. Liu, W.Y. Shi, H.X. Zhang, R. Zhou, X.H. Qin, Preparation of hydrophobic zeolitic imidazolate framework-71 (ZIF-71)/PVDF hollow fiber composite membrane for membrane distillation through dilute solution coating, Separ. Purif. Technol. 251 (2020) 117348.
[9] K.J. Lu, J. Zuo, T.S. Chung, Novel PVDF membranes comprising n-butylamine functionalized graphene oxide for direct contact membrane distillation, J. Membr. Sci. 539 (2017) 34–42.
[10] Z.C. Xiao, R. Zheng, Y.J. Liu, H.L. He, X.F. Yuan, Y.H. Ji, D.D. Li, H.B. Yin, Y. B. Zhang, X.M. Li, T. He, Slippery for scaling resistance in membrane distillation: a novel porous micropillared superhydrophobic surface, Water Res. 155 (2019) 152–161.
[11] W.A.F. Wae AbdulKadir, A.L. Ahmad, O.B. Seng, N.F. Che Lah, Biomimetic hydrophobic membrane: a review of anti-wetting properties as a potential factor in membrane development for membrane distillation (MD), J. Ind. Eng. Chem. 91 (2020) 15–36.
[12] M. Rezaei, D.M. Warsinger, J.H. Lienhard V, M.C. Duke, T. Matsuura, W. M. Samhaber, Wetting phenomena in membrane distillation: mechanisms, reversal, and prevention, Water Res. 139 (2018) 329–352.
[13] W. Wu, X. Zhang, L. Qin, X. Li, Q. Meng, C. Shen, G. Zhang, Enhanced MPBR with polyvinylpyrrolidone-graphene oxide/PVDF hollow fiber membrane for efficient ammonia nitrogen wastewater treatment and high-density Chlorella cultivation, Chem. Eng. J. 379 (2020) 122368.
[14] F. Li, J. Meng, J. Ye, B. Yang, Q. Tian, C. Deng, Surface modification of PES ultrafiltration membrane by polydopamine coating and poly(ethylene glycol) grafting: morphology, stability, and anti-fouling, Desalination 344 (2014) 422–430.

[15] H. Li, H. Liu, W. Shi, H. Zhang, R. Zhou, X. Qin, Preparation of hydrophobic zeolitic imidazolate framework-71 (ZIF-71)/PVDF hollow fiber composite membrane for membrane distillation through dilute solution coating, Separ. Purif. Technol. 251 (2020) 117348.
[16] Z. Xu, Z. Liu, P. Song, C. Xiao, Fabrication of super-hydrophobic polypropylene hollow fiber membrane and its application in membrane distillation, Desalination 414 (2017) 10–17.
[17] L. Zou, P. Gusnawan, Y.B. Jiang, G.Y. Zhang, J.J. Yu, Macrovoid-inhibited PVDF hollow fiber membranes via spinning process delay for direct contact membrane distillation, ACS Appl. Mater. Interfaces 12 (2020) 28655–28668.
[18] G. Navascues, P. Tarazona, Contact angle and line tension dependence on curvature, Chem. Phys. Lett. 82 (1981) 586–588.
[19] A.H. Barber, S.R. Cohen, H.D. Wagner, External and internal wetting of carbon nanotubes with organic liquids, Phys. Rev. B 71 (2005) 115443.
[20] N.T. Hassankiadeh, Z. Cui, J.H. Kim, D.W. Shin, A. Sanguineti, V. Arcella, Y.M. Lee, E. Drioli, PVDF hollow fiber membranes prepared from green diluent via thermally induced phase separation: effect of PVDF molecular weight, J. Membr. Sci. 471 (2014) 237–246.
[21] M. Ghidiu, M.R. Lukatskaya, M.Q. Zhao, Y. Gogotsi, M.W. Barsoum, Conductive two-dimensional titanium carbide 'clay' with high volumetric capacitance, Nature 516 (2014) 78–81.
[22] T. Zhang, L.Z. Zhang, Development of a MXene-based membrane with excellent anti-fouling for air humidification-dehumidification type desalination, J. Membr. Sci. 641 (2022) 119907.
[23] J.Q. Zhao, Y.W. Yang, C.H. Yang, Y.P. Tian, Y. Han, J. Liu, X.T. Yin, W.X. Que, A hydrophobic surface enabled salt-blocking 2D Ti_3C_2 MXene membrane for efficient and stable solar desalination, J. Mater. Chem. A 6 (2018) 16196–16204.
[24] Q.W. Su, J.Y. Zhang, L.Z. Zhang, Fouling resistance improvement with a new superhydrophobic electrospun PVDF membrane for seawater desalination, Desalination 476 (2020) 114246.
[25] D. Lohse, X.H. Zhang, Surface nanobubbles and nanodroplets, Rev. Mod. Phys. 87 (2015) 981–1035.
[26] C.A. Ward, J. Wu, Effect of contact line curvature on solid-fluid surface tensions without line tension, Phys. Rev. Lett. 100 (2008) 256103.
[27] J. Zhang, J.D. Li, M. Duke, Z. Xie, S. Gray, Performance of asymmetric hollow fiber membranes in membrane distillation under various configurations and vacuum enhancement, J. Membr. Sci. 362 (2010) 517–528.
[28] G.P. Li, L.Z. Zhang, Investigation of a solar energy driven and hollow fiber membrane-based humidification-dehumidification desalination system, Appl. Energy 177 (2016) 393–408.
[29] X.Y. Wang, Q.Q. Li, J.F. Zhang, H.M. Huang, S.Y. Wu, Y. Yang, Novel thin-film reverse osmosis membrane with MXene $Ti_3C_2T_x$ embedded in polyamide to enhance the water flux, anti-fouling and chlorine resistance for water desalination, J. Membr. Sci. 603 (2020) 118036.
[30] Q.W. Su, H. Lu, J.Y. Zhang, L.Z. Zhang, Fabrication and analysis of a highly hydrophobic and permeable block GO-PVP/PVDF membrane for membrane humidification-dehumidification desalination, J. Membr. Sci. 582 (2019) 367–380.
[31] L.Z. Zhang, Q.W. Su, Performance manipulations of a composite membrane of low thermal conductivity for seawater desalination, Chem. Eng. Sci. 192 (2018) 61–73.
[32] M.M. Ding, H. Xu, W. Chen, G. Yang, Q. Kong, D. Ng, T. Lin, Z.L. Xie, 2D laminar maleic acid-crosslinked MXene membrane with tunable nanochannels for efficient and stable pervaporation desalination, J. Membr. Sci. 600 (2020) 117871.
[33] F. Liu, C.H. Du, B.K. Zhu, Y.Y. Xu, Surface immobilization of polymer brushes onto porous poly(vinylidene fluoride) membrane by electron beam to improve the hydrophilicity and fouling resistance, Polymer 48 (2007) 2910–2918.
[34] Z. Xu, Y.Q. Sun, Y.X. Zhuang, W.H. Jing, H. Ye, Z.F. Cui, Assembly of 2D MXene nanosheets and TiO_2 nanoparticles for fabricating mesoporous TiO_2